ECS The Electrochemical Society
Advancing solid state & electrochemical science & technology

Review—Phosphor Plates for High-Power LED Applications: Challenges and Opportunities toward Perfect Lighting

Review—Phosphor Plates for High-Power LED Applications: Challenges and Opportunities toward Perfect Lighting

Yoon Hwa Kim, Noolu S. M. Viswanath, Sanjith Unithrattil, [ORCID] **Ha Jun Kim, and Won Bin Im**[*,z]

School of Materials Science and Engineering and Optoelectronics Convergence Research Center, Chonnam National University, Buk-gu, Gwangju 61186, Korea

In the past decades, solid-state lighting based on phosphors as energy converters has been a fast-growing industry. Phosphor-converted white light-emitting diodes (pc-wLEDs) enable high-power applications and miniaturization; for this, the phosphor must have good stability and high efficiency. In order to satisfy this demand, phosphor plates have been proposed instead of conventional organic-based phosphor binders. In this review, such phosphor plates are categorized according to their synthesis methods, and the advantages and disadvantages of each category are detailed. In addition, we describe the major aspects of phosphor plates that require improvement for applications in high-power devices. For the fabrication of high-power LEDs, the phosphor configuration, color purity, porosity, and particle size of glass powders are key properties to enhance the luminescence efficiency and reduce the generation of heat inside wLED packages, thereby improving thermal stability.

The advent of authentic, energy-efficient lighting in the home and workplace significantly affected the modern way of life. Beginning with the mass production of incandescent light bulbs, and with the subsequent evolution of fluorescence lights, lighting technology has developed rapidly in the last few decades. Since Edison's incandescent bulb in 1879,[1] artificial lighting has been developed to increase power output and decrease the size of the system. The development of red light-emitting diodes (LEDs) in 1962[2] and blue LEDs in 1993[3] allowed innovation in lighting and display. In particular, combinations of blue LEDs and yellow phosphors are used for many applications because they can realize cheap and efficient white solid-state lighting with several advantages including long lifetimes, eco-friendly behavior, and the capacity of miniaturization.[4–6]

In phosphor-converted white LEDs (pc-wLEDs), the phosphor converter dispersed in silicon resin (phosphor-in-silicon; PiS) is directly packed on a blue InGaN chip.[7] When driven by a bias current, the emitted blue light absorbed by the phosphor is emitted as yellow light; together with the transmitted blue light, this constitutes white luminescence. However, this method lacks a red component, which entails the drawbacks of a poor color rendering index (CRI) and limited correlated color temperature (CCT). To overcome these drawbacks, one proposed method mixes yellow phosphors with phosphors having green to red emissions under blue excitation.[8] In pc-wLEDs, the color is primarily determined by the ratio of the blue emission from the LED chip to the yellow to red emission from the phosphor. However, the efficacy and brightness are determined by the converted yellow to red emission, as it contributes the bulk of lumens. In this configuration, the heat generated from the LED chip and phosphor cannot be efficiently dissipated because of the poor thermal stability and weak thermal conductivity of the resin, which causes luminous decay and color shifting in white light-emitting diodes (wLEDs).[9] When the temperature of the wLED is increased by the driving current of the LED chip, color degradation occurs because of the thermal quenching properties of the phosphor.[10] The thermal stability of white lighting has been particularly important because of the recently proposed laser-driven white lighting. To avoid this color degradation, many methods have been proposed, such as coatings on the phosphor surface,[11,12] solid solutions of phosphor compositions,[13–15] and phosphor plates.[16,17] Among these proposed methods, interest has grown in phosphor plates with
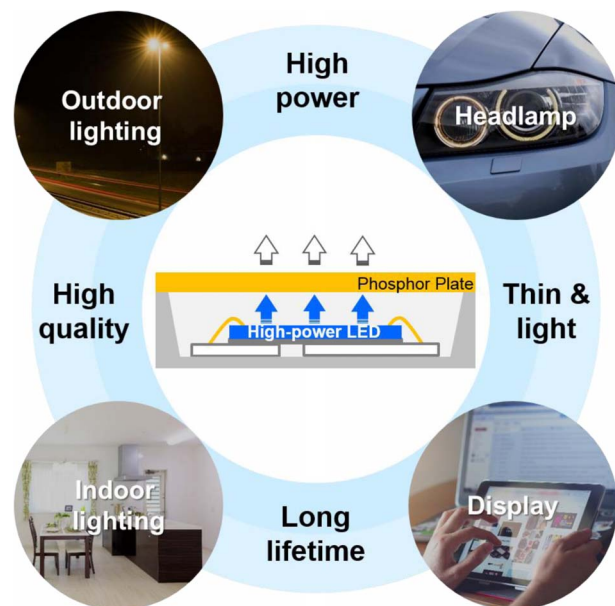

Figure 1. Schematic of white light-emitting diodes based on phosphor plate and their applications.

high efficiency, reproducibility, and mass productivity. In addition, the unique properties of phosphor plates allow their potential use as high-brightness sources in automotive headlamps, projection, and search lamps, among other applications.

Phosphor plate converters have advantages over PiS including reduced degradation, reduced light scattering, and efficient heat removal. The ceramic plates have certain desirable optical properties in chip-converter assemblies because of their microstructures, as shown in Fig. 1. Early phosphor plates have been introduced to increase the efficiency of wLEDs. Narendran et al.[17] investigated glass plates coated with different densities of $Y_3Al_5O_{12}:Ce^{3+}$ (YAG:Ce^{3+}) phosphor to increase the light output and luminous efficacy (LE) by extracting backscattered light. Luo et al.[18] developed the "phosphor-on-top" configuration using a different geometry for the encapsulant. LE was improved by 7.8% compared to conventional polymer-based wLEDs.

It was demonstrated that phosphor plates showed improved thermal stability and high-humidity resistance in wLEDs by Fujita et al.[19] as actively studied by many researchers.

Phosphor plates of various types have been introduced by different researchers. Currently, five approaches are used, as categorized by the production method: phosphor ceramic plate (PCP), phosphor glass plate (PGP), glass phosphor plate (GPP), single-crystal phosphor plate (SCPP), and phosphor-in-glass (PiG). PCP produces a thin, transparent ceramic by sintering at high temperature and high pressure. In PGP, a co-precipitated phosphor is sintered in vacuum or a composition for forming a phosphor phase such as YAG:Ce^{3+} is sintered in glass at high temperature and high pressure. GPP is a glass matrix containing fluorescent substances crystallized under heat-treatment. SCPP uses the Czochralski method based on the phosphor composition. Finally, PiG use sintered mixtures of glass frit and phosphor.

Recently, Raukas et al.[20] reviewed the properties and preparation methods for LED phosphors and compared their performances. Chen et al.[21] reviewed the synthesis routes that provide transparent glass-ceramic phosphors and summarized the materials design and structure/properties optimization. However, details on plate phosphors for high-power applications are rarely discussed. In this article, we focus on the different methods used to fabricate phosphor plates to replace conventional polymer-based wLEDs (PiS), mainly PiG, and thereafter provide a detailed discussion on controlling synthesis parameters for high-power applications, such as color quality, pores in the plates, and the particle sizes of the phosphor and glass. We conclude by summarizing future directions of research related to phosphor plates for high-power applications.

Types and Characteristics of Phosphor Plates

This section describes the type and the representative results of phosphor plates and is not comprehensive about the current state-of-the-art.

Phosphor ceramic plate (PCP) and phosphor glass plate (PGP).—In this section, we classify PCP and PGP. PCP are produced as thin, transparent ceramics by sintering at elevated temperature and high pressure. PGP involve the production of glass phase by melting the raw material powders and extracting phosphor crystal phase within the glass matrix through annealing. In both of these plate types, synthesis does not involve use of phosphor powers; instead, raw materials to prepare the phosphor composition are mixed with the raw materials for the glass material.

PCPs are a relatively new entrant in the color conversion plates and are still being investigated. Commercially viable technologies were developed by Philips/Lumileds and Osram.[20] Studies on PCP mainly focus on the YAG:Ce^{3+} phosphor. In 2008, Bechtel et al.[22] reported YAG:Ce^{3+}-based PCP for pc-wLEDs. They introduced a thin-film flip-chip wLED with a PCP named Lumiramic that was later commercialized by Philips. In order to control the emission characteristics of PCP, it is necessary to control the thickness and the concentration of Ce^{3+}. Nishiura et al.[23] reported on a transparent YAG:Ce^{3+}-based PCP produced by the co-preparation method. It was heated at $1780°C$ for 20 h under vacuum. They measured the thickness dependency of LE in YAG:Ce^{3+}-based PCP. Waetzig et al.[24] prepared translucent, polycrystalline YAG:Ce^{3+}-based PCP with different concentrations of Ce^{3+} and different PCP thicknesses. The intensities of the absorption bands of PCP were changed with increasing specimen thicknesses and concentrations of Ce^{3+} ions. They optimized the PCP by decreasing the thickness or the Ce^{3+} ion content, allowing the preparation of wLEDs with a CCT of 5000 K and LE of 76.6 lm W^{-1}.

Cozzan et al.[25] prepared a blue $BaMgAl_{10}O_{17}$:Eu^{2+}-based PCP using microwave-assisted heating and spark plasma sintering. Wang et al.[26] reported a green MgAlON:Eu^{2+}-based PCP. Joshi et al.[27] fabricated a thin transparent yellow α-SiAlON:Eu^{2+}-based PCP. For enhanced optical properties, Y_2O_3 was added to the PCP and the concentration of Eu^{2+} was controlled. Raukus et al.[20] demonstrated an amber $M_2Si_5N_8$:Eu^{2+}-based PCP developed at Osram Sylvania.

Li et al.[28,29] fabricated a red CaSiAlN$_3$:Eu^{2+} (CASN:Eu^{2+})-based PCP. Analysis techniques such as cathodoluminescence (CL), transmission electron microscopy, and electron probe micro-analysis were employed to provide new insight on the systems. Analysis showed that the phosphor particles had core–shell structures. The core of the structure caused the strong red light emission owing to the comparable refractive index to that of shell. The crystal structure evolution from CASN through CASN–Si_2N_2O to Ca-α-SiAlON is shown in Fig. 2a. The overall emission of the system was attributed to the core, as the shell acted like a quenching center because of the defects present in it. This is shown in Fig. 2b. The correlation between the thickness of the translucent ceramic plate and the transmittance was studied for three representative thicknesses (0.150, 0.329, and 0.476 mm) as shown in Fig. 2c. The strong red emission of the PCP under 441 nm blue laser excitation is shown in Fig. 2d. Fig. 2e shows the effect of blue laser power density on the luminous flux. At a fixed power density, the thin plate (0.150 mm) maintains a higher LE than the thick one (0.467 mm). The thermal stability and conductivity of the PCP were superior to those of the corresponding powder phosphor.[29]

To improve the required characteristics of the PCP, other materials can be added to the raw materials during the synthesis process. Ji et al.[30] and Lee et al.[31] reported $Lu_3Al_5O_{12}$:Ce^{3+} (LuAG:Ce^{3+})-based PCPs made from inorganic materials such as SiO_2 and AlN. Ji et al. reported that the addition of SiO_2 was not helpful for improving the luminescence properties and even lowered the photoluminescence (PL) intensity, while MgO enhanced the luminesce properties. Lee et al. fabricated LuAG:Ce^{3+}-based PCP with different amounts of AlN and Al_2O_3 in the PCP as sintering aids. When AlN was added, the optical and thermal properties were increasingly deteriorated with increasing amounts of AlN. However, the PCP with Al_2O_3 showed improved thermal stability upon increasing the amount of Al_2O_3, although the optical properties were negatively affected.

Fujita et al.[19] introduced a YAG:Ce^{3+}-based PGP prepared by melting and annealing SiO_2–Al_2O_3–Y_2O_3. A translucent glass plate with microcrystalline phosphor particles dispersed in it was obtained. The LE and stability of the wLED fabricated using the YAG:Ce^{3+}-based PGP were compared with those of PiS-type wLEDs. The YAG:Ce^{3+} PGP showed improved properties and was recommended as a candidate for the realization of resin-free, stable, and long-lifetime wLED applications. Song et al.[32] reported a YAG:Ce^{3+}-based PGP for high-power laser diodes (LDs). They used LDs and nanoscale YAG:Ce^{3+}-based PGPs for white light generation in automotive lighting and compared the nanoscale phosphor with the bulk-sized YAG:Ce^{3+} phosphor. Both the luminous flux and conversion efficiency of the YAG:Ce^{3+}-based PGP were improved compared to those of the bulk-size YAG:Ce^{3+} phosphor. The results indicated that the PGP was a good candidate for use in high-power applications. However, it was difficult to control the crystallinity of the phosphor phases in the glass plates.

Many studies have been conducted to improve the synthesis process at high temperatures and high pressures. Wang et al.[33] prepared a YAG:Ce^{3+}-based PGP with low SiO_2 contents by flame spray-quenching and hot press sintering. The intensity of the emission spectra was increased with decreasing SiO_2 contents. Huang et al.[34] reported on YAG:Ce^{3+}-based PGP synthesized via spontaneous crystallization, which had the advantages of easy fabrication, low cost, and a short production period. They optimized the PGP based on thickness and the concentration of Ce^{3+}. Chen et al.[35] fabricated a YAG:Ce^{3+}-based PGP employing tape-casting. Sai et al.[36] reported a YAG:Ce^{3+}-based PGP grown by the optical floating zone technique. Liu et al.[37] reported a YAG:Ce^{3+}-based PGP grown by horizontal directional solidification method.

White lighting devices produced based on this method still suffered from low CRIs and high CCTs because of the lack of red emission. In addition, the phosphor material compositions that can be utilized in this technique are limited. Furthermore, detailed study is necessary to adjust the crystallization rate and crystal composition. To overcome these disadvantages, many researchers investigated PGPs with various emission colors. Nakanishi and Tanabe[38] obtained an Eu^{2+}-doped PGP
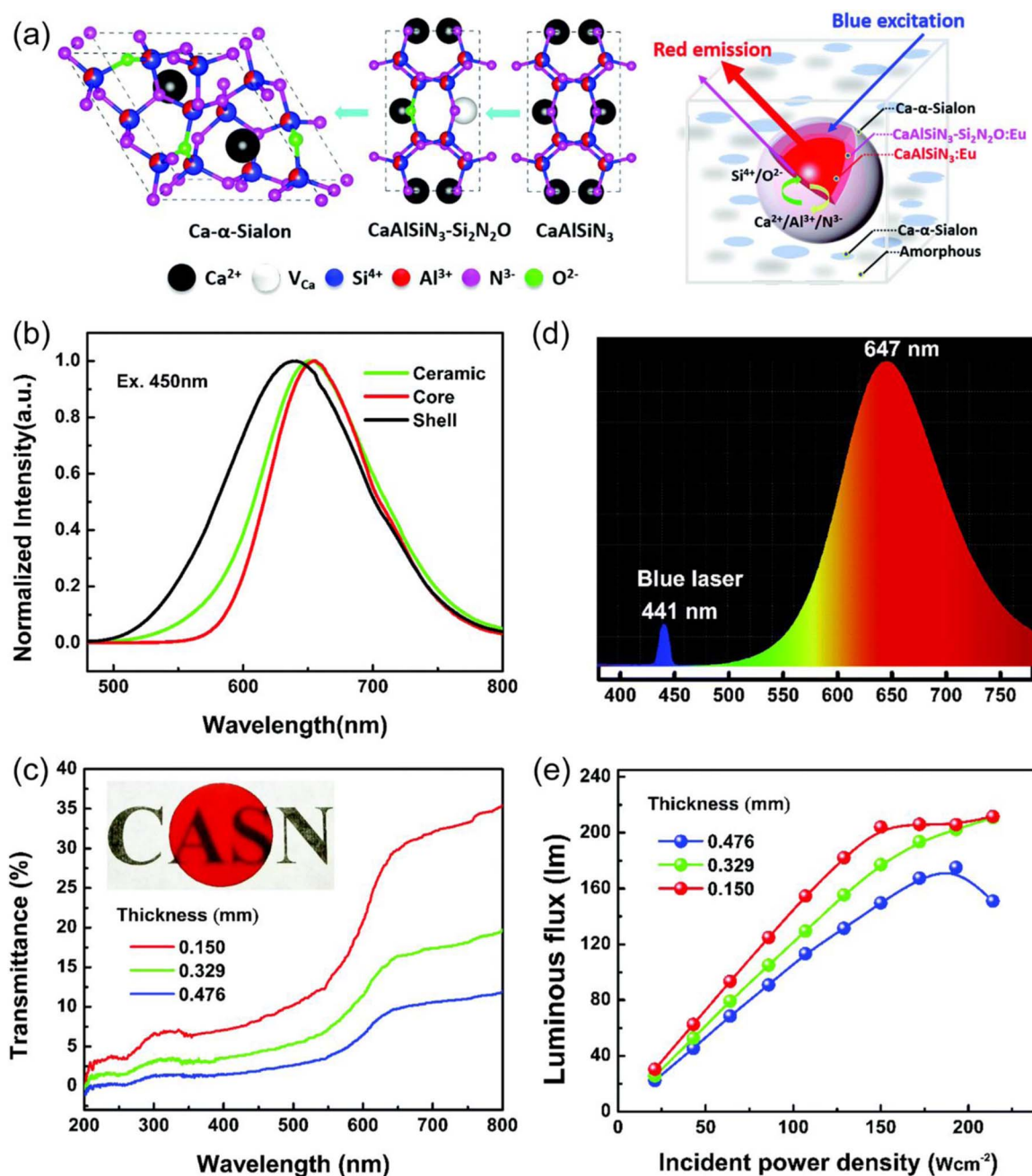
Figure 2. (a) (left) Crystal structure evolutions from $CaAlSiN_3$ through $CaAlSiN_3$–Si_2N_2O to Ca-α-SiAlON. (right) A schematic illustrating the core–shell composite microstructure and the luminescence process in such a microstructure. (b) The emission spectra of the phosphor ceramic, the core, and the shell. The data for the shell is based on our study of the $CaAlSiN_3$–Si_2N_2O:Eu^{2+} phosphor powders ($Ca_{1-x}Al_{1-x}Si_{1+x}N_{3-x}O_x$, $x = 0.22$).[103] (c) The in-line transmittance spectra of the phosphor ceramic with three different thicknesses; inset shows the photograph of 0.150-mm-thick phosphor on a black character. (d) The luminescence spectrum of the $CaAlSiN_3$:Eu^{2+} phosphor ceramic (0.150 mm thickness) under the excitation of the 441-nm blue laser. (e) The effects of blue laser densities on the luminous fluxes. (Adapted from Ref. 29. Copyright 2017 Royal Society of Chemistry.)

in which two phosphor crystals with green and red emission bands were present. They reported that the use of the CaO–SiO_2 system as the host glass obtained a PGP having broad emission bands for good color rendering. The Ca_2SiO_4:Eu^{2+}–$Ca_3Si_2O_7$:Eu^{2+}-based PGP showed a broad emission band from 490 nm to 700 nm. Cui et al.[39] reported a $SrSiO_3$:Eu^{2+},Sm^{3+}-based PGP, which had a broad PL excitation spectrum applicable to an ultraviolet (UV) LED chip. They obtained a white-emitting PGP under UV excitation by controlling the molar ratio of Eu^{2+}/Sm^{3+} in the PGP.

PCP and PGP are advantageous in that it is unnecessary to prepare a separate phosphor and allow molding in various forms. When total conversion of blue light from the monochromatic sources are needed, unlike phosphor-in-silicone mixes, where a much thicker phosphor powder-silicone body is used above the LED, PCP offers significantly lower optical losses due to the dense continuous body. Also, the lower activator content in the PCP results in a lower thermal quenching and would ensure better performance at high operating temperature.[20] However, for these methods, the phosphor composition, which must
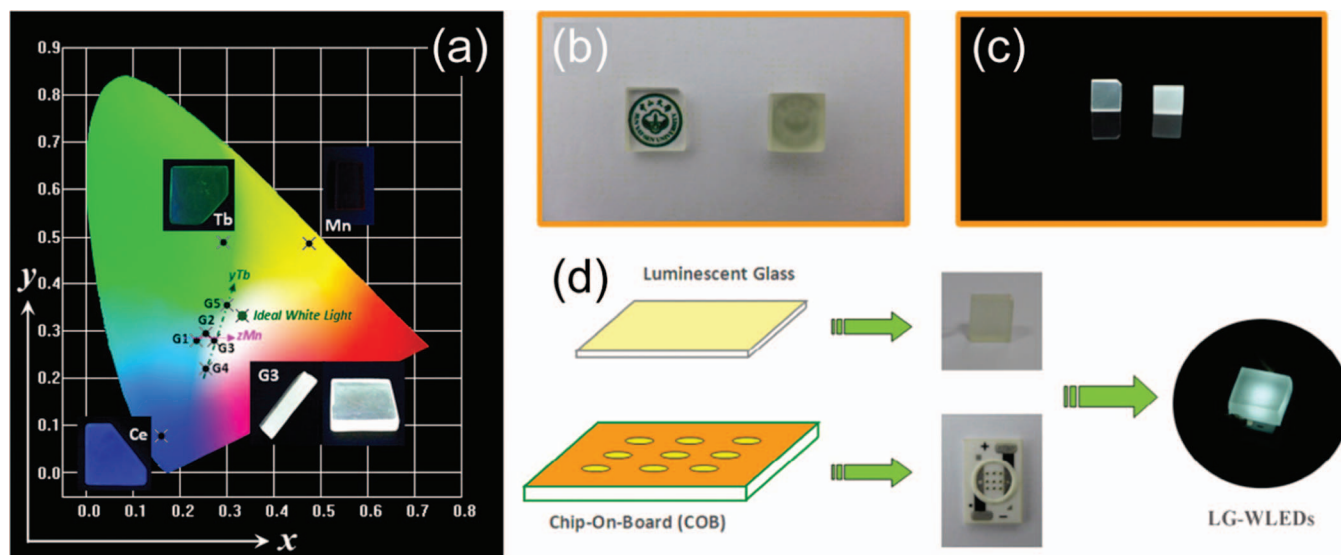
Figure 3. (a) CIE chromaticity diagram of SLSAKP:0.3%Ce^{3+}, SLSAKP:1.0%Tb^{3+}, SLSAKP:0.5%Mn^{2+}, and SLSAKP:0.3%Ce^{3+},yTb^{3+},zMn^{2+} glasses (G1: $y = 2.0\%$, $z = 0.5\%$; G2: $y = 2.0\%$, $z = 1.0\%$; G3: $y = 2.0\%$, $z = 2.0\%$; G4: $y = 1.0\%$, $z = 2.0\%$; G5: $y = 4.0\%$, $z = 2.0\%$). Inset shows digital photographs of SLSAKP:0.3%Ce^{3+}, SLSAKP:1.0%Tb^{3+}, SLSAKP:0.5%Mn^{2+}, and SLSAKP:0.3%Ce^{3+},2.0%Tb^{3+},2.0%Mn^{2+} glasses under 365-nm UV lamp irradiation. (b,c) Photographic images of (left) the mirror- and (right) the rough-polished SLSAKP:0.3%Ce^{3+},2.0%Tb^{3+},2.0%Mn^{2+} glasses: (b) under white-emitting fluorescent lamp; (c) under 365-nm UV lamp. (d) The conceptual and actual fabrication process of LG-wLEDs based on combination of COB and luminescent glass. (Reprinted with permission from Ref. 43. Copyright 2014 American Chemical Society.)

be easy to realize in liquid phase, is limited. The methods are also disadvantageous in that scattering control of the blue light source is required depending on the thickness and crystal phase.

Glass phosphor plate (GPP).—GPP is a kind of phosphor plate containing active ions or luminescent materials capable of emitting light within glass materials for light conversion. The glass itself serves as the phosphor. Active ions in the glass matrix can include rare earth ions such as Eu^{2+}, Eu^{3+}, and Ce^{3+}, in addition to Pr^{3+}, Nd^{3+}, Sm^{3+}, and Tm^{3+} and transition metals such as Mn^{2+}, Sn^{2+}, Cr^{2+}, and Cr^{3+}. Since GPP can directly convert color through the glass material without needing separate phosphors, the manufacturing process for GPP is simple and economical. In addition, it is advantageous for free formation depending on the characteristics of the glass material. After the GPP was first reported by Qiu et al.,[40] various combinations of active ion compositions and glass media were found to produce emissions in the entire range of the visible spectrum.

Many researchers have focused on the composition of the glass matrix. Generally, the quantum efficiency (QE) of active ions in the glass matrix increases with decreasing phonon energy, but GPPs with lower phonon energies have weaker chemical and mechanical stabilities. That is, common silicate-based glass materials have excellent chemical, mechanical, and thermal stability, but the QE of the active ions is very limited because of the high phonon energy. Zhou et al.[41] presented a Bi^{3+}-doped alkali borosilicate glass with the composition SiO$_2$–B$_2$O$_3$–Na$_2$O–Al$_2$O$_3$. The synthesis process involved soaking the dry porous glasses in solutions of Bi(NO$_3$)$_3$ for two days; the Bi^{3+}-doped nanoporous glass was produced by treating it in a special atmosphere of air and Ar. The sample treated in Ar was observed to have two emission bands, centered at 465 nm and 590 nm, under 280 nm excitation. The combination of these two bands covered the full visible spectrum, generating broadband white-light emission. Rocha et al.[42] reported a Ce^{3+}/Eu^{2+},Eu^{3+} co-doped silica aluminosilicate glass. This GPP showed a broad yellow emission band centered at 550 nm under excitation by a 405 nm laser, reaching the QE of 26%. These results indicated the possibility of color converting materials for full-spectrum white lighting. Zhang et al.[43] reported Ce^{3+},Tb^{3+},Mn^{2+}-doped single-composition tunable white-emitting silicate SiO$_2$–Li$_2$O–SrO–Al$_2$O$_3$–K$_2$O–P$_2$O$_5$

glasses (SLSAKP:Ce^{3+},Tb^{3+},Mn^{2+}), and discussed in detail the energy transfer from Ce^{3+} to Tb^{3+} and Mn^{2+}. Fig. 3a shows the International Commission on Illumination (CIE) chromaticity diagram of SLSAKP:Ce^{3+},Tb^{3+},Mn^{2+} depending on changes in activator ions. Fig. 3c illustrates the schematic and actual fabrication process of GPP-based wLEDs based on the UV chip-on-board (COB) configuration.[43] Zhang et al.[44] reported an Eu^{2+}-doped silicate SLSAKP GPP, which had a tunable emission band. Gao et al.[45] used Al powder to reduce Eu^{3+} to Eu^{2+} in a SiO$_2$–Al$_2$O$_3$–Na$_2$CO$_3$–YF$_3$–NaF glass matrix. They found that the ratio of Eu^{3+} to Eu^{2+} could be controlled by using various amounts of Al. The ratio of Eu^{3+} to Eu^{2+} was also found to change during the heating and homogenization processes.

Silicate compositions and various other compositions such as borates, phosphates, and aluminates have been applied to produce GPPs. As in the previous studies, researchers have focused on controlling color and efficiency by manipulating the active ions in the glass. Edgar et al.[46] reported a fluorobromozirconate glass doped with Eu^{2+}/Ce^{3+}. Lakshminarayana et al.[47] reported Tm^{3+}/Dy^{3+} co-doped oxyfluoride germinate glasses for white light emission. Loos et al.[48] reported a GPP emitting various colors from different energy transfers between Tb^{3+} and Eu^{3+} ions. The energy transfer from Tb^{3+} to Eu^{3+} was translated into the position of the chromaticity coordinates moving further into the orange/red region under 376 nm and 485 nm excitation as shown in the Fig. 1 of Reference 48.

The ability to realize various wavelengths in a single plate using active ions is one great advantage of GPP. However, GPPs are disadvantageous in that the local structure capable of maximizing the conversion efficiency of active ions is limited compared to that of general phosphor plates; in addition, the crystal field distribution is heterogeneous and the light conversion efficiency is extremely low. In the case of active ions having excellent LE in GPPs, the excitation light source is usually UV in wavelength, and there is a limitation for suitable sources in high-power applications excited near 400 nm and 450 nm.

Single-crystal phosphor plate (SCPP).—SCPPs are presently the optimal white-source converters, particularly for high-brightness applications. Regarding good general lighting devices, high efficiency, good thermal stability, and long-term reliability are necessary. The
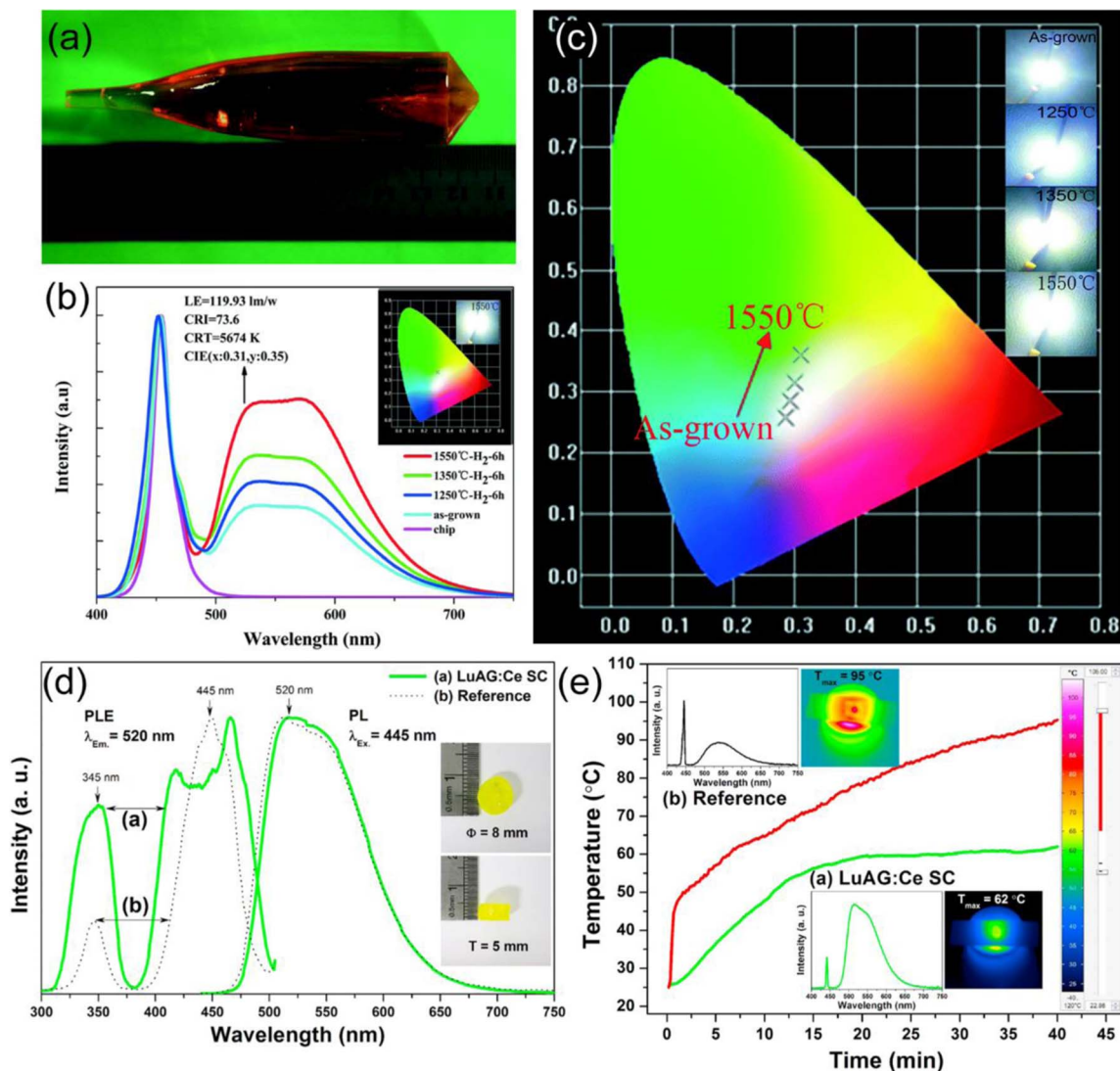
Figure 4. (a) As-grown Ce,Mn:YAG single crystal grown by the Czochralski method. (b) White luminescence spectra of the WLED fabricated with a blue InGaN chip and the annealed Ce,Mn:YAG single crystal at 1550°C. Inset: the image of a WLED at an operating current of 20 mA. (c) CIE color coordinates of the Ce,Mn:YAG single crystal wafers at different temperatures. The insets show the luminescence photographs of the Ce,Mn:YAG single crystal wafer-based WLEDs at an operating current of 20 mA. (Reprinted with permission from Ref. 49. Copyright 2015 Royal Society of Chemistry.) (d) 520-nm monitored PLE and 445-nm excited PL spectra of the single-crystal LuAG:Ce^{3+} phosphor (a; green solid lines) and polycrystalline powder phosphor as a reference (b; black dot lines). Insets show photographs of the single crystal with a diameter (Ø) of 8 mm and a thickness (T) of 5 mm. (For interpretation of the references to color in this figure legend, the reader is referred to the web version of this article.) (e) Thermograph spectra as a function of time of (a) the LuAG:Ce^{3+} single crystal and (b) reference powder at the laser-irradiated spot of 6.5 mm in diameter of a 445-nm blue LD with an output optical power of 5 W under an operating voltage of 4.7 V and forward-bias current of 3.6 A. The insets show each emission spectrum and thermograph image after 40 min operation of the blue LD. (Reprinted with permission from Ref. 53. Copyright 2017 Royal Society of Chemistry and American Chemical Society.)

advantages of SCPP include maneuverability by optimizing the preferred geometric and optical parameters through simple mechanical methods like polishing and slicing. This allows SCPPs to fit into specific designs with enhanced light harvesting.

The SCPP based on YAG single crystal was investigated by Gu et al.[49] In this, YAG:Ce^{3+},Mn^{2+} single crystal is grown by the Czochralski method using a [111] oriented single crystal as seed. A transparent crystal of about 15 mm in diameter with bright red coloration is obtained as shown in Fig. 4a. The crystal on annealing at 1550°C attained a LE of about 119.93 lmW^{-1} and a CRI of 73.6 at a CCT of 5674 K as shown in Fig. 4b. Annealing performed at various temperatures under H$_2$ atmosphere improves the luminescence properties of the as-grown crystal and displaced the CIE color coordinates of the wLED units as shown in Fig. 4c.[49] The SCPP for white lighting was also investigated by Latynina et al.[50] They fabricated a Y$_3$Al$_5$O$_{12}$:Ce^{3+},Gd^{3+}-based SCPP using the Czochralski method,

grown along the <111> direction. The current dependence of LE for the 0.5 mm-thick SCPP-based wLED under 455 nm excitation is indicated in the Fig. 8 of the Reference 50. The SCPP-based wLED was decreased in LE from 175 lm W^{-1} to 136 lm W^{-1}, while the commercial phosphor powder showed almost twice this reduction in performance.[50] Martin et al.[51] measured the optical properties of YAG:Ce^{3+}-based SCPPs with different dopant concentrations under different sample temperatures. Salimian et al.[52] examined the possibility of using YAG:Ce^{3+}-based SCPP as potential targets for light generation via LDs. They reported that YAG:Ce^{3+}-based SCPPs were potentially usable in future high-brightness lighting devices.

A similar garnet LuAG:Ce^{3+} was studied as an SCPP for use in high-power applications. Kang et al.[53] investigated a green LuAG:Ce^{3+}-based SCPP for high-power laser lighting. A LuAG:Ce^{3+} SCPP with diameter (Ø) of 8 mm and thickness (T) of 5 mm is shown in Fig. 4c. An improvement in the photoluminescent emission

Table I. Summary of the phosphor plate characteristics.

	PCP	GPP	SCPP	PiG
Luminous flux	○	△	◎	△
Thermal stability	◎	○	◎	○
Color matching	△	◎	△	◎
Cost	○	◎	△	◎
Reliability	◎	◎	◎	◎
Manufacture	○	◎	△	◎
Thermal conductivity[a] [W m^{-1}K^{-1}]	5–13[100]	~1[101]	8–11[102]	~1[101]

*△: bad, ○: good, ◎: best.
[a]The thermal conductivity of PiS is 0.1-0.2 W m^{-1}K^{-1}.[100]

intensity of the LuAG:Ce^{3+} SCPP at the 345 nm peak by a factor of 3.7 in comparison with the reference is obtained. This improvement is attributed to the reduced defects near the second-lowest $5d^1$ level in the single crystal. This SPCC had a higher optical density of 92% and a lower QE of 63% under 445 nm excitation compared to the polycrystalline reference sample having values of 88% and 90%, respectively. This is from the absence of light-scattering sources, such as grain boundaries or surface roughness, within the single crystal. Fig. 4d shows the thermography spectra as a function of time for the single-crystal LuAG:Ce^{3+} phosphor. The insets of the figure show the emission spectrum and thermographic image at thermal equilibrium. In this device, the heat locally generated at the point of irradiation is easily dissipated because of the absence of interfacial air layers. The lower equilibrium temperature of 62°C after operating the blue LD for 40 min compared to the 95°C obtained for the powder samples illustrates this. Thus, laser lighting using the LuAG:Ce^{3+} SPCC as a color converter can produce stable light emission under the high operating current used in such devices.[53]

Hence, SCPPs showed significantly better stability and high LE and are therefore important candidates for replacing resin-based wLEDs. The notable advantage of a SCPP versus a transparent PCP is an enhanced thermal conductivity. (Refer Table I) However, SCPPs use sophisticated synthesis methods to obtain optically transparent plates for the application, which renders the process expensive and low in reproducibility, thus hindering commercial production. SCPP may also suffer from manufacturing issues due to variable dopant concentrations in a given crystal boule.[54] Because of the waveguide loss and backward emission loss, the QE and easy extraction of phosphor plates are lower than those of commercial powder phosphors.[50] Furthermore, the SCPP configuration requires further investigations on the dependence of structural and morphological features on the luminescence performances under high-power operation.

Phosphor-in-glass (PiG).—PiG structures are composed of commercial phosphors and glass frits and are commonly synthesized by co-sintering a mixture thereof at optimal conditions. At a certain temperature, the viscosity of the glass increases dramatically. This condition is used to produce a high packing ratio. In order to manufacture PCP and SCPP, high pressure and high temperatures of 1200°C or more are required. However, PiG can be sintered at atmospheric pressure and fired below 800°C. The processing conditions are determined by the properties of the phosphor and glass frit materials; therefore, PiG can be fabricated using relatively simple processes compared to other phosphor plate types. This is advantageous in that mass production and economic efficiency can be secured. In particular, PCP and SCPP are limited to phosphor systems that can be sintered or melt-processed, while PiG can freely use various high-efficiency phosphors. In addition, it is possible to manufacture various shapes with free shape control, and it is easy to control the color coordinates by controlling the thickness and mixing ratio of phosphors. Therefore,

it is clear that PiG provides good processing flexibility and simplicity compared to SCPP and PCP counterparts.

The composition of the glass constituting the PiG is important in determining the LE. As the glass melts, the phosphor particles require excellent heat resistance to maintain their original properties; the refractive indexes of the phosphor and the glass matrix must also be similar to diminish backlight scattering and retain PiG transparency. Therefore, increasing attention has been given to low-melting-temperature glasses for the dispersion of phosphors.

Allen et al.[55] investigated the YAG:Ce^{3+} phosphor in a SiO$_2$–PbO glass matrix (Schott SF57 glass). PbO-based PiG shows a favorable refractive index, but the Pb content can cause environmental pollution issues. Therefore, many researchers have focused on Pb-free glasses with good optical properties and synthesis conditions. Segawa et al.[56] reported borate and tellurite (TeO$_2$) glasses dispersing Ca-α-SiAlON:Eu^{2+} phosphors, sintered at 1000°C and 500°C, respectively. They compared the optical properties of the borate and tellurite glasses according to changes in the glass compositions. The borate glass-based PiG had high optical transparency, but sintering temperatures reaching 750°C, which limits the use of some phosphor compositions like CASN:Eu^{2+}, which begins degrading at 600°C. A tellurite glass containing the phosphors formed TeO$_2$ crystals when the glass was melted at 700°C. This indicates that tellurite-based PiG has the lowest sintering temperature of glass-based phosphors. Huang et al.[57] fabricated YAG:Ce^{3+} PiGs using these properties of tellurite glass. They investigated a one-step melt-quenching technique (OSMQ). In this method, the tellurite-based glass powders (TeO$_2$–ZnO–K$_2$O–B$_2$O$_3$–Bi$_2$O$_3$) were mixed with YAG:Ce^{3+} phosphor and sintered at the relatively low temperature of 520°C. The absorption at 460 nm was stronger in the conventional PiG than in the OSMQ-PiG. It was found that the sintering temperature and time had significant effects on the luminescence properties of the phosphor. The measured LE of wLEDs based on OSMQ-PiG reached 125 lm W^{-1} with a CCT of 4329 K, and the corresponding CRI of 68.

Silicate-based glass is highly abundant and suitable for PiG. Lee et al.[58] developed PiG from SiO$_2$–B$_2$O$_3$–RO (R = Ba,Zn)-based glass frits and YAG:Ce^{3+} powders by sintering at 750°C for 30 min. The report detailed glass systems and the transmittance of silicate glass depending on the sintering conditions. The control of the ratio of YAG:Ce^{3+} phosphor to glass frits for obtaining the targeted color coordinates of wLEDs was also discussed. They found that increased phosphor content corresponded to improved yellow emission intensity and concluded that the emission intensity and the color coordination must be balanced to obtain targeted wLEDs. Chen et al.[59] developed PiG through spreading multiple phosphors within a SiO$_2$-based glass (SiO$_2$–Na$_2$O–Al$_2$O$_3$–CaO) at 680°C. They sintered the glass frits with various phosphor compositions, including YAG:Ce^{3+}, LuAG:Ce^{3+}, and CASN:Eu^{2+}. The transparency and quantum yield of the YAG:Ce^{3+}- and LuAG:Ce^{3+}-based PiG barely changed, but those of CASN:Eu^{2+}-based PiG were decreased as the sintering temperature increased. They analyzed the properties of the CASN:Eu^{2+}-based PiG depending on sintering temperature via differential thermal analysis (DTA), X-ray diffraction (XRD), and high-resolution transmittance electron microscopy (HRTEM) in detail. It was confirmed that the crystalline temperature (T_x) of the CASN:Eu^{2+} phosphor was 696°C using DTA, and XRD of CASN:Eu^{2+}-based PiG showed that high sintering temperatures exceeding T_x weakened the crystalline phase of the CASN:Eu^{2+} phosphor in the glass matrix. Interdiffusion between the CASN:Eu^{2+} phosphor and SiO$_2$ from the glass in the CASN:Eu^{2+}-based PiG was analyzed through HRTEM. Similar interdiffusion was also observed in YAG:Ce^{3+}-based PiGs.[60] These results indicate that it is essential to develop a glass composition with a low sintering temperature.

Sb-based glass can be processed by low-temperature sintering. Zhang et al.[61] developed a transparent YAG:Ce^{3+}-based PiG using Sb-based glass. They prepared a precursor glass of Sb$_2$O$_3$–B$_2$O$_3$–TeO$_2$–ZnO–Na$_2$O–La$_2$O$_3$–BaO thoroughly mixed with commercial YAG:Ce^{3+} phosphors and sintered the mixture at 540–690°C for 10–80 min. The synthesis conditions were optimized for PiG with 5 wt%

YAG:Ce^{3+} phosphor depending on the measured transparency, PL, and quantum yield of samples. The optimized sintering conditions were reported as 570°C and 20 min. The PiG-based wLED yielded a LE of 124 lm W^{-1}, a CCT of 6674 K, and a CRI of 70 under 350 mA. Chen et al.[62] developed a transparent YAG:Ce^{3+}-based PiG with a high quantum yield of 94% and improved thermal quenching properties using Sb$_2$O$_3$-based glass (Sb$_2$O$_3$–ZnO–K$_2$O–B$_2$O$_3$). The fabricated PiG based wLED exhibited a high LE of 130 lm W^{-1}, a CCT of 5298 K, and a CRI of 65, under an operating current of 350 mA.

As aforementioned, a new glass composition for preventing the recrystallization of the phosphor was proposed by Lee et al.[63] They fabricated PiG with glass frits based on the SiO$_2$–Na$_2$O–RO system, which has the low sintering temperature of 550°C. No remarkable thermal degradation of CASN:Eu^{2+} was observed with the SiO$_2$–Na$_2$O–RO glass. Zhu et al.[64] proposed a red-emitting PiG synthesized by dispersing CASN:Eu^{2+} phosphor in a ZnO–B$_2$O$_3$–BaO–Al$_2$O$_3$ glass matrix.

PiG has been actively developed because it can meet various demands through process design and accommodate various phosphors by lowering the glass formation temperature. Therefore, not only YAG:Ce^{3+}-based PiG but also PiG with phosphors of various emission wavelengths have been reported by many researchers. Lee et al.[65] reported the feasibility of using PiG as an encapsulant for highly unstable SrGa$_2$S$_4$:Eu^{2+} sulfide phosphors, which were not previously used in wLED applications because of high chemical instability. Zhu et al.[66] developed a green PiG using β-SiAlON:Eu^{2+} phosphor under various blue laser flux densities. The PiG was prepared by mixing the β-SiAlON:Eu^{2+} phosphor with ZnO–B$_2$O$_3$–BaO–Al$_2$O$_3$ glass frits. The thermal stabilities of the PiG materials were investigated and compared with those of the phosphor powder. The temperature-dependent PL intensity of both samples declined linearly with increasing temperature. Yoshimura et al.[67] attempted to prepare β-SiAlON:Eu^{2+}-based PiG using a silica glass. The PiG was exposed to blue laser light with a power density of 8 W mm^{-2}, and compared to a PiS. The area of the phosphor-containing silicone resin that was irradiated by laser changed from green to black in color, although the green emission from the PiG remained stable after irradiation for 60 s. This indicated that the PiG had high durability under high-power light.

For use in high-power applications, PiG, which consists of a single phosphor, can be controlled in properties by varying the concentration of the phosphor in the glass matrix and the thickness of the plate, as is done with other phosphor plates. Zhang et al.[68] reported a YAG:Ce^{3+}-based PiG fabricated through a conventional melting method. Precursor glasses with the composition of SiO$_2$–Al$_2$O$_3$–B$_2$O$_3$–ZnO–BaO were used for the purpose. The mixtures were sintered for 30 min at 700°C. They reported a YAG:Ce^{3+}-based PiG with a high blue COB as shown in Fig. 5a. The dependence of the amount of YAG:Ce^{3+} phosphor in PiG on the electroluminescence (EL) spectra of PiG-based wLEDs is shown in Fig. 5b. All EL spectra are normalized to the blue emission from the COB LED to explore spectral variations. The emission intensity from the YAG:Ce^{3+} phosphor centered at 550 nm is increased with increasing amounts of YAG:Ce^{3+} phosphor in the PiG. In Fig. 5c, the color coordinates of the wLEDs are shifted from cool white to normal white and, finally, to yellow with increasing amounts of the YAG:Ce^{3+} phosphor. The optimized phosphor content in the PiG based on the CCT is 3 wt%. The wLED fabricated using this concentration has a high LE of 92 lm W^{-1}, a CCT of 5414 K, and CRI of 68.4.[68] Chen et al.[69] reported a modified YAG composition, YAG:Ce^{3+},Mn^{2+},Si^{4+} with improved red component, incorporated into TeO$_2$–B$_2$O$_3$–ZnO–Na$_2$O–Al$_2$O$_3$ based low-melting glass. This combination offers a homogeneous dispersion of phosphor in the matrix owing to the similar density and refractive index of the materials and thereby a reduced back scattering. The samples were prepared with varying thickness from about 0.5 to 1.2 mm and the corresponding EL spectra and the shift in CIE color coordinate when operated under 350 mA forward current is shown in Fig. 5d. The CIE color

coordinates of the PiG based wLED were blue shifted on increasing the driving current as shown in Fig. 5e. When operated for longer duration by maintaining at 150°C, the LE loss of the PiG based wLED unit was 11.2% while the loss is 19.3% for a similar PiS based wLED. The comparison of the percentage loss in LE of both the samples are shown in Fig. 5e. Also, no considerable changes in other luminescence parameters like CCT, CRI and CIE were detected.[69] Zhang et al.[70] developed a transparent YAG:Ce^{3+}-based PiG. A thick film was coated on a glass substrate with the composition of TeO$_2$–B$_2$O$_3$–ZnO–Na$_2$O–Al$_2$O$_3$ through a screen-printing process. They employ YAG:Ce^{3+}-based PiG thick films at the bottom side of the glass substrate, which contributes to the improvement of the luminance value by enhancing the efficacy of blue-light photon excitation. The luminous intensity of the yellow emission region is enhanced monotonically as the film thickness increases. The emissive colors shift from blue to white and then to yellow, consistent with their actual luminescence photographs shown in the inset. The LE intensifies with increasing film thickness, while both CCT and CRI decrease, which is ascribed to the increased absorption of blue light and emission of yellow light by the YAG:Ce^{3+}-based PiG thick films. The optimal sample yields an LE of 78.7 lm W^{-1}, a CCT of 5612 K, and a CRI of 70.2.[70]

We summarize the overall performances of the phosphor plates in Table I. The above PiG method works well in high-power white lighting, but there is a limit in improving the quality of lighting. Therefore, in Perspective and summary section, we discuss the control factors for phosphor plates to produce high-quality high-power white lighting.

Aspects of Improvement for High-Power Applications

Methods to improve color quality.—Color quality is an important consideration for phosphor-converted white lighting systems as general illumination sources. The CCT and CRI are important parameters that determine the color quality of light sources for general illumination. The CCT essentially quantifies the color whiteness of a light source. This metric relates the appearance of a light source to the appearance of a theoretical black body heated to a high temperature and characterizes the color of the emitted light, not the color of illuminated objects.[71] The CRI characterizes how the source interacts with its environment; the ability to accurately render all colors by a full-spectrum source such as sunlight is defined as 100. Values approaching 100 indicate that a real object looks similar under the illumination source to what is seen under natural light.[72] In this section, we review the methods available to improve color quality and summarize the most important color issues related to phosphor plate-converted white lighting systems. Three major types of improvements are suggested: (1) mixing rare earth ions in the plate itself or phosphor composition, (2) mixing two or more phosphor compositions with glass frit, and (3) modifying the plate design.

The strategy of addition of rare earth ions to enhance the CRI and control the CCT has been used throughout phosphor plates. Cui et al.[39] designed Eu^{2+}/Sm^{3+} co-doped silicate glass by high-temperature melting under a reducing atmosphere and obtained Eu^{2+}/Sm^{3+} co-doped SrSiO$_3$ PCP by heat-treatment. They found broad emission peaks from 400 nm to 550 nm, since Eu^{2+} occupied two kinds of Sr^{2+} sites, as well as several sharp emission peaks at 563 nm, 600 nm, and 713 nm, associated with the transitions of Sm^{3+} under 365-nm excitation. Tunable emission color by varying the Sm^{3+} concentration was achieved because of the energy transfer from Eu^{2+} to Sm^{3+} ions. Yi et al.[73] reported on PiG prepared from a mixture of YAG:Ce^{3+} phosphor and high-refractive-index glass frits containing Eu^{3+} and Mn^{2+} ions. The CCT of the emitted white light was shifted from ∼7000 K to 4244 K by controlling the concentration of Eu^{3+} ions in the YAG:Ce^{3+}-based PiG. Warm white light generation with a CCT of 4014 K was realized by a specimen containing 0.3 mol% Mn^{2+} ions in the YAG:Ce^{3+}-based PiG. Zhou et al.[74] fabricated PiG containing YAG:Ce^{3+} phosphor and Eu^{3+} ions in order to improve the CCT and CRI. They realized various CIE color coordinates using YAG:Ce^{3+}-based PiG by controlling the amount of YAG:Ce^{3+} phosphor and the
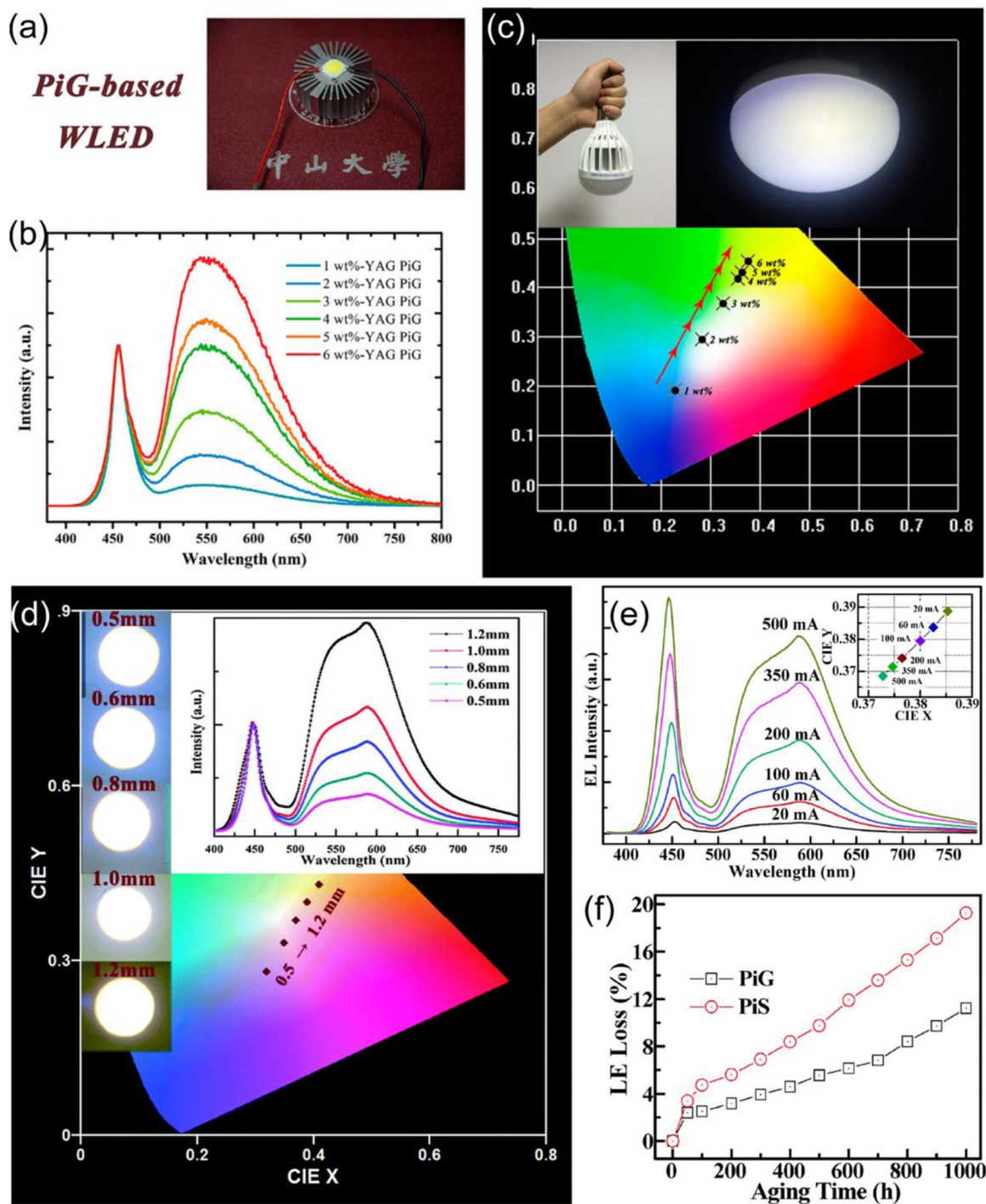
Figure 5. (a) Prototype of the YAG-based wLED; (b) Normalized EL spectra; and (c) CIE color coordinates of PiG-based wLEDs with different YAG concentrations; insets of (c) shows the lamp device photographs of the PiG-based wLEDs in operation and under a 300 mA forward current. (Reprinted with permission from Ref. 67. Copyright 2017 American Chemical Society.) (d) CIE coordinates of the YAG:0.06Ce^{3+},0.05Mn^{2+},0.05Si^{4+} PiG-based LED devices with various thicknesses under a 350 mA driving current, insets show the corresponding EL spectra and the luminescence photographs in operation. (e) EL spectra of the fabricated PiG-based w-LEDs under the current regulation (20–500 mA), the inset shows the variation of the CIE chromaticity coordinates operated under different forward bias currents. (f) LE loss of the PiG- and PiS-based warm w-LEDs with aging time prolonging for 1000 h at 150°C. (Reprinted with permission from Ref. 68. Copyright 2015 Royal Society of Chemistry.)

concentration of Eu^{3+} ions in PiG. They reported the corresponding wLED fabrication using optimal conditions to show a LE of 122 lm W^{-1}, a CCT of 6532 K, and a CRI of 75. Park et al.[75] studied PiG fabricated with Eu^{3+}- and Pr^{3+}-doped SiO$_2$-B$_2$O$_3$-*R*O glass by embedding yellow YAG:Ce^{3+} phosphor. They reported improved CRI values in the YAG:Ce^{3+}-based PiG with 1 mol% Eu$_2$O$_3$ (CCT 6066

K, CRI 70.2) and Pr$_2$O$_3$ (CCT 7884 K, CRI 73.6) and compared these to the bare sample (4810 K, CRI 64.7). In this method, a rare earth ion with a specific emission wavelength is added during the synthesis of the plate to simplify the process. In a similar manner, a full-color white-emitting phosphor can be prepared by adding rare earth ions to phosphor compositions, and then the phosphor is used to fabri-

cate a plate. Feng et al.[76] obtained a YAG:Ce^{3+},Pr^{3+},Cr^{3+}-based PC with a white color tuned by controlling the concentration of rare earth ions. The optimized PC, located around the theoretical white point of (0.33, 0.33), achieved a LE of 67.3 lm W^{-1} and a CRI of 72. Chen et al.[69] reported a chromaticity-tunable PiG fabricated by co-sintering YAG:Ce^{3+},Mn^{2+},Si^{4+} phosphor and TeO_2–B_2O_3–ZnO–Na_2O–Al_2O_3 glass frits. They reported the glass composition with the optimal transmittance and mixed it with YAG:Ce^{3+},Mn^{2+},Si^{4+} phosphor to produce PiG with improved thermal properties. The optimized PiG with YAG:$0.06Ce^{3+}$,$0.05Mn^{2+}$,$0.05Si^{4+}$ phosphor achieved a LE of 64.96 lm W^{-1}, CCT of 6818 K, and CRI of 79.8 under a driving current of 350 mA. There have also been reports on other phosphor compositions having full-color white emission being used to prepare phosphor plates. For example, Zhang et al.[77] investigated a PiG fabricated from a mixture with $Ca_9Gd(PO_4)_7$:Eu^{2+},Mn^{2+} multiple-emission phosphors and SiO_2–Al_2O_3–B_2O_3–ZnO–BaO glass frit. They argued that the PiG based on single-component full-color emitting phosphor had shown excellent thermal quenching behavior and good humidity-resistance performance compared with PiS. The COB-type wLED of $Ca_9Gd(PO_4)_7$:Eu^{2+},Mn^{2+}-based PiG reached the CCT of 3283 K under 120 mA driving current. However, these results showed that the method had limited utility because the substitution of rare earth ions for the glass matrix or the phosphor could control the CCT or improve the CRI, but only with a reduced LE, because of the energy transfer between the rare earth ions.

In these three kinds of systems, those utilizing mixtures of two or three phosphors are the most frequent, especially in PiG, and also efficient. Such mixtures are achieved by mixing well-known commercial phosphors such as YAG:Ce^{3+} and CASN:Eu^{2+} to produce white emission. Han et al.[78] reported a PiG prepared from a sintered mixture of silicate-based glass, YAG:Ce^{3+} phosphor, and CASN:Eu^{2+} phosphor, which did not show thermal degradation of the constituent phosphors. They found the glass composition for preventing recrystallization of CASN:Eu^{2+} phosphor and successfully fabricated a wLED with the best combination of each phosphor, which had a CCT of 3789 K and a CRI of 93. Ahn et al.[79] employed a PiG with a low sintering temperature based on the SiO_2–P_2O_5–ZnO system. A thick film of commercial CASN:Eu^{2+} and YAG:Ce^{3+} phosphors was applied using a screen-printing method. They reported a warm wLED with the LE of 98.95

lm W^{-1}, CCT of 3497 K, and CRI of 89.1 achieved by altering the ratio of the two phosphors in the glass matrix. In addition, a white color-emitting plate can be obtained by mixing various phosphor compositions other than well-known phosphors. Zhong et al. and Wang et al. fabricated PiGs based on newly developed $La_{0.5}Na_{0.5}TiO_3$:Eu^{3+} phosphor,[80] $La_2Ti_2O_7$:Eu^{3+} phosphor,[81] and $CaMg_2Al_{16}O_{27}$:Mn^{4+} phosphor[82] with the commercial YAG:Ce^{3+} yellow phosphor. These red phosphors were proposed to solve the recrystallization problem. In these cases, the CCTs of the PiG-based wLEDs evolved from cool white to warm white and the CRIs were increased depending on the amounts of red phosphor. In order to minimize interactions between phosphor with different compositions, Wang et al.[83] proposed a garnet-based PiG based on the $Y_3Mg_2AlSi_2O_{12}$:Ce^{3+} orange phosphor and $Y_3Al_{4.6}Ga_{0.4}O_{12}$:$Ce^{3+}$ green phosphor in TeO_2-based glass. Although this method is simple, it has the limit of LE deterioration by reabsorption and interaction between phosphors.

In order to solve these problems, various designs of color-converting plates have been proposed. Pricha et al.[84] and Peng et al.[85] investigated layered plates by screen-printing methods. The YAG:Ce^{3+} PC with layered CASN:Eu^{2+} phosphor was disadvantageous as an efficient optical converter. This was because of the chemical interactions and ion diffusion at the interface during heat-treatment, which minimized the number of active centers and caused distortions within the host lattice that reduced the luminescence activity of the phosphor system. The combination of R-G-B phosphors proposed for use along with UV LED showed no reabsorption between phosphors based on the order in which the layers were fabricated, but a decrease in CRI was observed. To minimize these phenomena, Kim et al.[86] proposed a one-step fabrication of a horizontal two-layered and four-quadrant PiG for eliminating the reabsorption of the emitted green light by the red phosphor of high-power wLEDs. The reported design eliminated the interfacial layers through the one-step process and thereby avoided scattering losses at the interfaces. Digital photographs of the one-step fabricated PiGs, schematics, and LEDs under operation are shown in Fig. 6a. The EL spectra of the combination under an operating bias current of 350 mA and the corresponding CIE chromaticity coordinates are shown in Figs. 6b and 6c, respectively. The report showed that the total emission intensity of the one-step fabricated PiG was enhanced by about 112%.[86] Peng et al.[87]
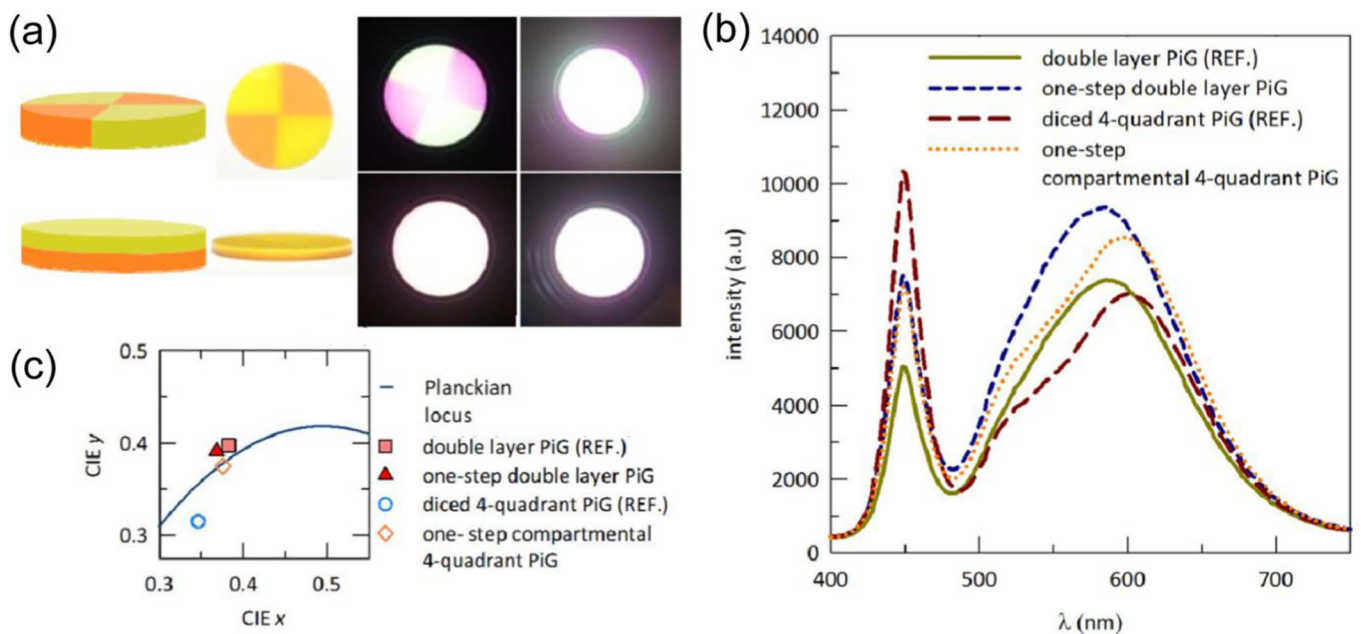

Figure 6. (a) An actual image of the one-step fabricated PiG, (b) EL spectra of the four configurations of the PiG-LED system, under operating conditions of 350 mA and 20 V, and (c) the CIE-1931 chromaticity coordinates of the corresponding wLED system. (Reprinted with permission from Ref. 85. Copyright 2016 Optical Society of America.)
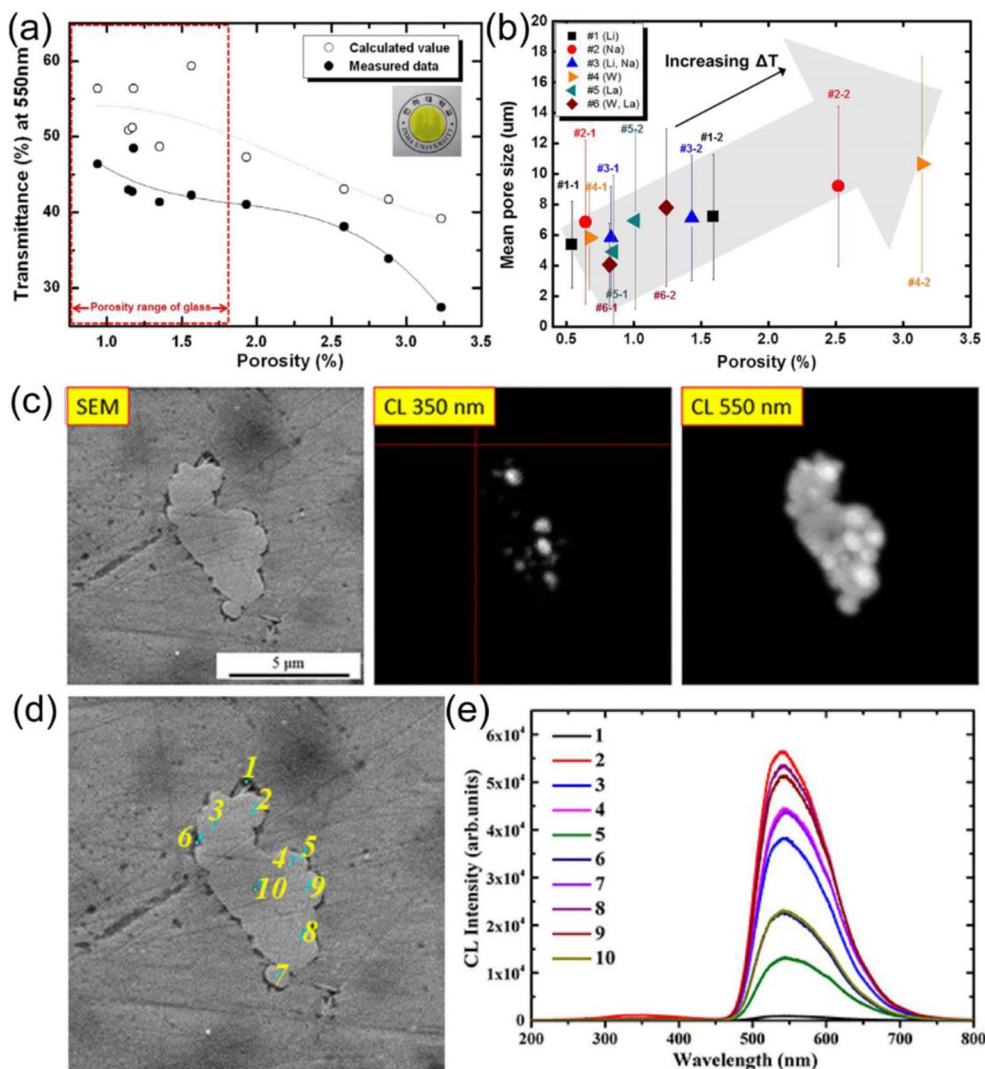
Figure 7. (a) Calculated and measured transmittance of PIG versus porosity. (Reprinted with permission from Ref. 91. Copyright 2015 Optical Society of America.) (b) Variation in mean pore size and porosity of PIGs. (Reprinted with permission from Ref. 92. Copyright 2015 Optical Society of America.) (c) SEM and CL mapping images emitting at 350 and 550 nm of 3 wt% YAG-PiG sample in the single particle; (d) SEM and (e) point CL spectra of 3 wt% YAG-PiG sample in a single particle. (Reprinted with permission from Ref. 67. Copyright 2017 American Chemical Society.)

proposed the facile preparation of patterned PiG in which YAG:Ce^{3+} and CASN:Eu^{2+} phosphors were arranged in the form of concentric rings. The experimental results indicated that LED units with the patterned PiGs yielded high LE and excellent color quality by reducing the reabsorption of yellow emission by red phosphors. The different colors emanating from the different parts of such arrangements are separately excited by blue radiation from the LED. In this arrangement, relative strengthening of the red component in the emission bands is observed when the number of concentric rings is increased. The increase in the area of the interfacial region between the red and yellow phosphors causes this increase of reabsorption of yellow emission by the red phosphor.[87]

Control of pore in phosphor plate and particle size of phosphor.—
In wLEDs, the residual porosity in the phosphor plate is a critical factor determining the efficacy, color coordinates, and color angular shift of the light emitted by the LED units. As a result of the sintering process, the porosity of the plate decreases and the transmission of the blue component increases. When the thickness of the plate is kept constant, this results in increased yellow emission until it reaches its peak value when the optimum absorption is attained.[88,89] Fujita et al.[90] evaluated the influence of light scattering on the LE of a YAG:Ce^{3+} phosphor

ceramic. The LE of the phosphor ceramic increased with increasing YAG:Ce^{3+} crystal size while the light scattering coefficient decreased. Kim et al.[91] developed a SrGa$_2$S$_4$:Eu^{2+}-based PiG microscale cube of ∼100 μm in dimensions that showed enhanced thermal stability and moisture resistance for wLED applications. They reported that the PiG microscale cubes were assembled based on the size and geometric conditions for scatter-free phosphors.

Kim et al.[92] studied the transmittance of PiG as a factor affecting the luminescence properties of wLEDs; transmittance relates closely to the residual pores of sintered glass. They investigated the correlation between the porosity and optical transmittance of sintered glass. As the porosity decreases, the transmittance and LE of the sintered glass plate increase, while the light scattering coefficient is decreased. With an increase in porosity, the transmittance decreases from 56.3% to 27.4% at 550 nm, as shown in Fig. 7a.[92] Kim et al.[93] investigated the interactions between blue light from an LED chip and pores within a PiG plate and the effect of light scattering on the optical properties. They investigated the pore characteristics of the PiG based on the viscosity of various glass compositions using the SiO$_2$–B$_2$O$_3$–ZnO system, low-glass-transition modifiers (Li$_2$O, Na$_2$O), and high-refractive-index modifiers (La$_2$O$_3$, WO$_3$). As the sintering temperature is increased, the viscosity is increased and the mean pore size
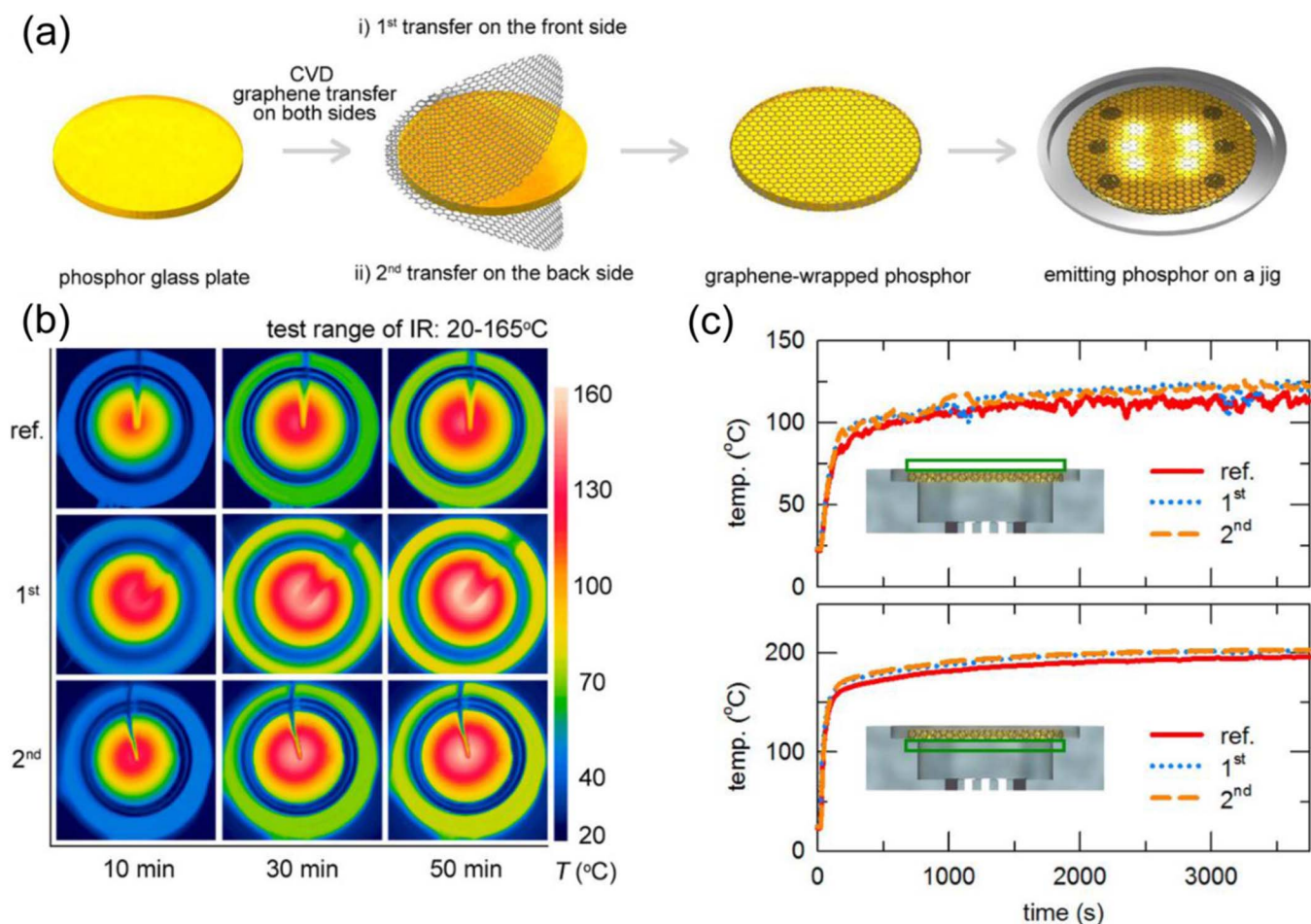
Figure 8. (a) Schematic showing the transfer of graphene from Cu foils to the phosphor-in-glass plates (PGP) by a poly(methyl methacrylate)-assisted transfer method. (b) Thermal imaging of the LEDs under operation after different operating times, and (c) temperatures on both surfaces (green rectangular domains) of the PGPs measured using a thermocouple as a function of the time of operation. (Reprinted with permission from Ref. 94. Copyright and 2016 American Chemical Society.)

and porosity are increased in every PiG sample, as shown in Fig. 7b; the increase in temperature is accompanied by pore coalescence and expansion.[93] Zhang et al.[68] reported a YAG:Ce^{3+}-based PiG and a detailed study on the interfacial structure between YAG:Ce^{3+} phosphor particles and the glass matrix by employing the combined technique of scanning electron microscope and in situ CL (SEM-CL). The CL mapping of 3 wt% YAG:Ce^{3+}-based PiG emitting at 550 nm is presented in Fig. 7c. The CL emission spectra of different points[1–10] on the YAG:Ce^{3+} particles have a prominent band at 550 nm and weak shoulder peaking at 350 nm with different relative intensities, as shown in Figs. 7d, 7e. The shoulder peak is attributed to the antisite defects in the YAG phosphor. This result indicates that the YAG:Ce^{3+} phosphor particles are intact in the powder.[68]

Dissipation of heat from driving white lighting.—The phosphor plate covers the LED package on the upper side of the wLED, which can confine the heat within the wLED when the phosphor plate is applied to high-power lighting sources. To overcome this problem, Song et al.[94] introduced a graphene-embedded red phosphor layer to satisfy the requirements for low CCT and high CRI values while conferring thermal stability. Graphene, having high thermal and electric conductivity, was applied to the phosphor plate for heat dissipation. They reported a thermally stable wLED with a CRI of 82, similar to those of bare phosphor plates. Kim et al.[95] developed a PiG for application in a remote-phosphor configuration of high-power wLEDs, in which a single layer of graphene was used to control the thermal characteristics of the PiG. Here, the degradation of luminescence by increase in

temperature was prevented by applying the single-layer graphene. The process of wrapping the PiG is shown in Fig. 8a. Both sides of the PGP were wrapped with chemical vapor deposition-fabricated graphene, and the wLED showed a 20% increase in LE through the effective heat dissipation through graphene. The graphene layer disperses the generated thermal energy; evaluation using thermal imaging with an infrared camera demonstrated that this heat is otherwise distributed on the surface of the PiG, as shown in Fig. 8b. The graphene-wrapped PiG shows a wider radial temperature gradient zone. The surface temperature of the PiG was increased to 100°C after 10 min and reached the maximum of 160°C after 30 min. This is due to the increase in the area over which heat was spread. The increase in area of spread made the convection process more effective. Fig. 8c shows the plot of temperatures as a function of time. The graphene-wrapped PiG shows temperatures 3.6−7.8% higher on the top surface compared to those on the bare PiG, indicating more effective heat transfer. Importantly, a major difference between the two color-converting plates is whether the graphene is wrapped or not, indicating that the graphene is important in maintaining the luminescent characteristics of the PiGs under high-power operations. Therefore, the proposed graphene-wrapped PiG is effective in maintaining the luminescence properties of the wLED during operation.[95]

The heat generated during the operation of a light source has attracted even more attention for LDs used as light sources. The heat from LDs is much greater than that from conventional LEDs, and therefore many researchers have proposed new heat-reducing designs. For example, Chang et al.[96] demonstrated a highly reliable
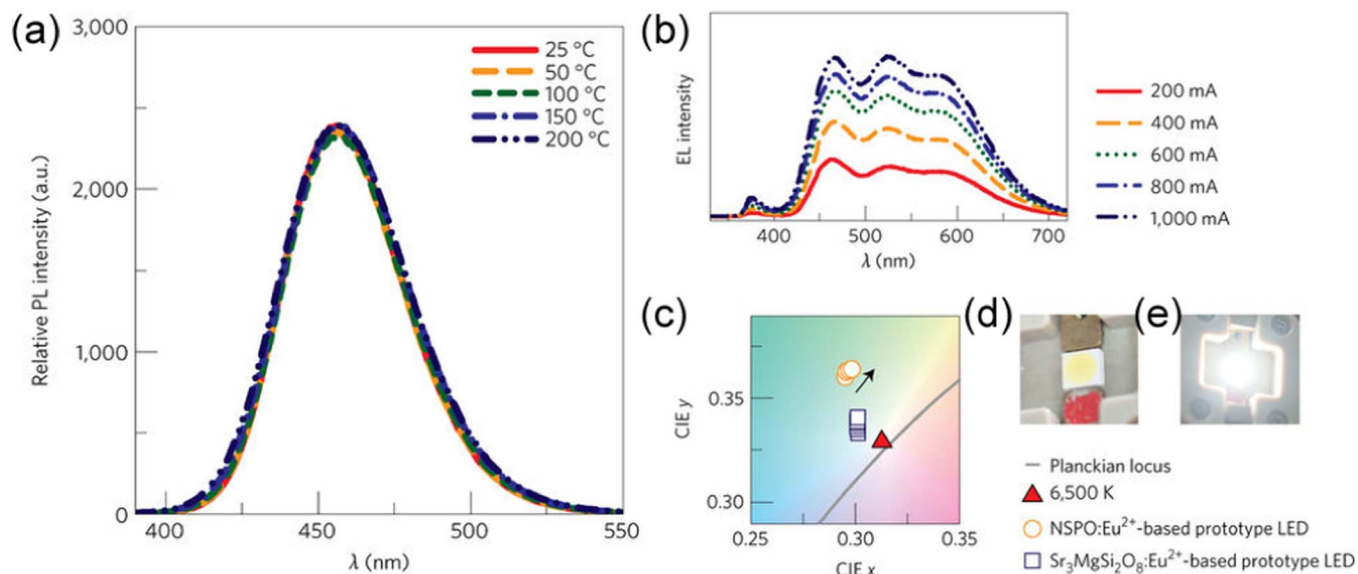
Figure 9. (a) Temperature-dependent emission spectra of $Na_{2.86}Sc_2(PO_4)_3$:0.07Eu^{2+} phosphor under 370 nm excitation in the temperature range 25–200°C with a temperature interval of 50°C. (b) EL spectra of WLED using $Na_{2.91}Sc_2(PO_4)_3$:0.03Eu^{2+} (NSPO:0.03Eu^{2+}) as the blue component. (c) CIE chromaticity coordinates of the fabricated NSPO:0.03Eu^{2+} prototype wLED compared to the commercial blue $Sr_3MgSi_2O_8$:Eu^{2+} phosphor-based wLED. (d,e) Image of the fabricated NSPO:0.03Eu^{2+} wLED prototype without (d) and with (e) an applied high flux operating current. (Reprinted with permission from Ref. 98. Copyright and 2017 Nature Publishing Group.)

glass-based color wheel in combination with a laser light engine for high-power laser-based operation. A demonstration of this design showed a thermal stability of approximately 14 times that of a silicone-based color wheel after high-power operation at 30 W_{opt} for 2000 h.

Perspective and Summary

In this review, we have presented different techniques employed in phosphor plate fabrication to improve the LE, thermal stability, and CCT control for high-power applications in white lighting. Through analyzing various experimental results, we conclude that the phosphor plate is a promising candidate for high-power applications in future and investigations on phosphor plate must be continued. Many areas require additional work, including but not limited to:

(1) Development of a simple synthesis method for improving color quality.
(2) Determination of optimal conditions by controlling pore and particle sizes in phosphor plate. Research on this area has been reported by several groups; more specific information is required on the phenomena occurring inside the phosphor plate.
(3) Replacement of glasses with thermally stable encapsulant materials such as Al_2O_3 and $MgAl_2O_4$ with YAG:Ce^{3+}. LDs, which have recently emerged as high-power lighting sources, provide peak efficiencies at much higher current densities and generate a lot of heat when driven. To survive this heat, the thermal conductivity of the phosphor plate must be further enhanced to promote heat dissipation and maintain a sufficiently low temperature of the phosphor. It is confirmed that a matrix with a high thermal conductivity is required to protect the phosphor powders when driven by white laser illumination. Therefore, phosphor plates with high thermal stability can be obtained by investigating and developing inorganic materials such as Al_2O_3 and $MgAl_2O_4$, as reported by certain groups.[97,98]
(4) Development of new PiG materials such as "zero-thermal-quenching phosphors" to overcome thermal stability issues. In addition to the matrix material of the phosphor plate, excellent chemical and thermal stability of the phosphors are required. The thermally insensitive phosphor reported by Kim et al.[99] of-

fers a new alternative to thermally stable color converters, as shown in Fig. 9. This phosphor has shown no thermal quenching even at 200°C; these characteristics are retained when applied to wLEDs. The phosphors with these properties are good candidates for making thermally stable phosphor plates.

Much progress has been made over the past decade in optimizing phosphor plates for application to white lighting. However, based on the scientific research and outlined experimental strategies, further efforts to improve color quality and stability and reduce costs remain necessary. This review provides a good summary benefiting the design and investigation of phosphor plates for potential use in high-power applications.

Acknowledgments

ORCID

Sanjith Unithrattil https://orcid.org/0000-0001-9072-7163

References

1. T. A. Edison, US223898 A, (1880).
2. M. G. Craford, R. D. Dupuis, M. Feng, F. A. Kish, and J. Laskar, *Proceedings of the IEEE*, **101**, 2154 (2013).
3. S. Nakamura, T. Mukai, and M. Senoh, *Applied Physics Letters*, **64**, 1687 (1994).
4. J. H. Oh, S. J. Yang, and Y. R. Do, *Light: Science & Applications*, **3**, e141 (2014).
5. T. Pulli, T. Donsberg, T. Poikonen, F. Manoocheri, P. Karha, and E. Ikonen, *Light: Science & Applications*, **4**, e332 (2015).
6. S. Nakamura, *MRS Bulletin*, **34**, 101 (2009).
7. S. Nakamura and G. Fasol, *The Blue Laser Diode: GaN Based Light Emitters and Lasers*, Springer (1997).
8. Y.-H. Won, H. S. Jang, K. W. Cho, Y. S. Song, D. Y. Jeon, and H. K. Kwon, *Optics Letters*, **34**, 1 (2009).
9. M. Hisashi, N. Shuji, and P. D. Steven, *Japanese Journal of Applied Physics*, **45**, L910 (2006).
10. J. Ueda, P. Dorenbos, A. J. J. Bos, A. Meijerink, and S. Tanabe, *The Journal of Physical Chemistry C*, **119**, 25003 (2015).

11. P. Arunkumar, Y. H. Kim, H. J. Kim, S. Unithrattil, and W. B. Im, *ACS Applied Materials & Interfaces*, **9**, 7232 (2017).
12. H. S. Yoo, W. B. Im, S. W. Kim, B. H. Kwon, and D. Y. Jeon, *Journal of Luminescence*, **130**, 153 (2010).
13. W. B. Im, N. George, J. Kurzman, S. Brinkley, A. Mikhailovsky, J. Hu, B. F. Chmelka, S. P. DenBaars, and R. Seshadri, *Advanced Materials*, **23**, 2300 (2011).
14. W. B. Im, N. N. Fellows, S. P. DenBaars, and R. Seshadri, *Journal of Materials Chemistry*, **19**, 1325 (2009).
15. W. B. Im, Y. Fourré, S. Brinkley, J. Sonoda, S. Nakamura, S. P. DenBaars, and R. Seshadri, *Optics Express*, **17**, 22673 (2009).
16. G. Harbers, S. Bierhuizen, and M. Pugh, US 7682850 B2, (2010).
17. N. Narendran, Y. Gu, J. P. Freyssinier-Nova, and Y. Zhu, *physica status solidi (a)*, **202**, R60 (2005).
18. H. Luo, J. K. Kim, E. F. Schubert, J. Cho, C. Sone, and Y. Park, *Applied Physics Letters*, **86**, 243505 (2005).
19. S. Fujita, S. Yoshihara, A. Sakamoto, S. Yamamoto, and S. Tanabe, in *Proc. SPIE 5941, Fifth International Conference on Solid State Lighting*, p. 594111 (2005).
20. M. Raukas, J. Kelso, Y. Zheng, K. Bergenek, D. Eisert, A. Linkov, and F. Jermann, *ECS Journal of Solid State Science and Technology*, **2**, R3168 (2013).
21. D. Chen, W. Xiang, X. Liang, J. Zhong, H. Yu, M. Ding, H. Lu, and Z. Ji, *Journal of the European Ceramic Society*, **35**, 859 (2015).
22. H. Bechtel, P. Schmidt, W. Busselt, and B. S. Schreinemacher, in *Proc. SPIE 7058, Eighth International Conference on Solid State Lighting*, p. 70580E (2008).
23. S. Nishiura, S. Tanabe, K. Fujioka, and Y. Fujimoto, *Optical Materials*, **33**, 688 (2011).
24. K. Waetzig, M. Kunzer, and I. Kinski, *Journal of Materials Research*, **29**, 2318 (2014).
25. C. Cozzan, M. J. Brady, N. O'Dea, E. E. Levin, S. Nakamura, S. P. DenBaars, and R. Seshadri, *AIP Advances*, **6**, 105005 (2016).
26. K. Li, H. Wang, X. Liu, W. Wang, and Z. Fu, *Journal of the European Ceramic Society*, **37**, 4229 (2017).
27. B. Joshi, Y. K. Kshetri, G. Gyawali, and S. W. Lee, *Journal of Alloys and Compounds*, **631**, 38 (2015).
28. S. Li, Q. Zhu, L. Wang, D. Tang, Y. Cho, X. Liu, N. Hirosaki, T. Nishimura, T. Sekiguchi, Z. Huang, and R.-J. Xie, *Journal of Materials Chemistry C*, **4**, 8197 (2016).
29. S. Li, D. Tang, Z. Tian, X. Liu, T. Takeda, N. Hirosaki, F. Xu, Z. Huang, and R.-J. Xie, *Journal of Materials Chemistry C*, **5**, 1042 (2017).
30. E.-K. Ji, Y.-H. Song, S. H. Bak, M. K. Jung, B. W. Jeong, D. B. Lee, and D.-H. Yoon, *Journal of Materials Chemistry C*, **3**, 12390 (2015).
31. M. J. Lee, Y. A. Roh, U. B. Humayoun, Y.-H. Song, and D.-H. Yoon, *Journal of Ceramic Processing Research*, **17**, 144 (2016).
32. Y. H. Song, E. K. Ji, B. W. Jeong, M. K. Jung, E. Y. Kim, and D. H. Yoon, *Scientific Reports*, **6**, 31206 (2016).
33. L. Wang, L. Mei, G. He, J. Li, and L. Xu, *Journal of the American Ceramic Society*, **94**, 3800 (2011).
34. J. Huang, X. Liang, W. Xiang, M. Gong, G. Gu, J. Zhong, and D. Chen, *Materials Letters*, **151**, 31 (2015).
35. J. Chen, H. Lan, Y. Cao, Z. Deng, Z. Liu, F. Tang, and W. Guo, *Journal of Alloys and Compounds*, **709**, 267 (2017).
36. Q. Sai and C. Xia, *Journal of Luminescence*, **186**, 68 (2017).
37. Y. Liu, M. Zhang, Y. Nie, J. Zhang, and J. Wang, *Journal of the European Ceramic Society*, **37**, 4931 (2017).
38. T. Nakanishi and S. Tanabe, *IEEE Journal of Selected Topics in Quantum Electronics*, **15**, 1171 (2009).
39. Z. Cui, R. Ye, D. Deng, Y. Hua, S. Zhao, G. Jia, C. Li, and S. Xu, *Journal of Alloys and Compounds*, **509**, 3553 (2011).
40. J. Qiu, Y. Shimizugawa, Y. Iwabuchi, and K. Hirao, *Applied Physics Letters*, **71**, 759 (1997).
41. S. Zhou, N. Jiang, B. Zhu, H. Yang, S. Ye, G. Lakshminarayana, J. Hao, and J. Qiu, *Advanced Functional Materials*, **18**, 1407 (2008).
42. A. C. P. Rocha, L. H. C. Andrade, S. M. Lima, A. M. Farias, A. C. Bento, M. L. Baesso, Y. Guyot, and G. Boulon, *Optics Express*, **20**, 10034 (2012).
43. X. Zhang, L. Huang, F. Pan, M. Wu, J. Wang, Y. Chen, and Q. Su, *ACS Applied Materials & Interfaces*, **6**, 2709 (2014).
44. X. Zhang, J. Wang, L. Huang, F. Pan, Y. Chen, B. Lei, M. Peng, and M. Wu, *ACS Applied Materials & Interfaces*, **7**, 10044 (2015).
45. Y. Gao, J. Qiu, and D. Zhou, *Journal of the American Ceramic Society*, **100**, 2901 (2017).
46. A. Edgar, J.-M. Spaeth, S. Schweizer, S. Assmann, P. J. Newman, and D. R. MacFarlane, *Applied Physics Letters*, **75**, 2386 (1999).
47. G. Lakshminarayana, H. Yang, and J. Qiu, *Journal of Solid State Chemistry*, **182**, 669 (2009).
48. S. Loos, M. Mungra, B. Ahrens, R. L. Leonard, A. Evans, J. A. Johnson, F. Steudel, and S. Schweizer, *Journal of Luminescence*, **187**, 298 (2017).
49. G. Gu, W. Xiang, C. Yang, and X. Liang, *CrystEngComm*, **17**, 4554 (2015).
50. A. Latynina, M. Watanabe, D. Inomata, K. Aoki, Y. Sugahara, E. García Víllora, and K. Shimamura, *Journal of Alloys and Compounds*, **553**, 89 (2013).
51. M. Rejman, V. Babin, R. Kucerková, and M. Nikl, *Journal of Luminescence*, **187**, 20 (2017).
52. A. Salimian, J. Silver, G. R. Fern, H. Upadhyaya, A. Metcalfe, T. G. Ireland, P. Harris, and R. Haghpanahan, *ECS Journal of Solid State Science and Technology*, **5**, R172 (2016).
53. T. W. Kang, K. W. Park, J. H. Ryu, S. G. Lim, Y. M. Yu, and J. S. Kim, *Journal of Luminescence*, 35 (2017).
54. A. P. Piquette, M. E. Hannah, and K. C. Mishra, *ECS Transactions*, **41**, 1 (2012).
55. S. C. Allen and A. J. Steckl, *Applied Physics Letters*, **92**, 143309 (2008).
56. H. Segawa, S. Ogata, N. Hirosaki, S. Inoue, T. Shimizu, M. Tansho, S. Ohki, and K. Deguchi, *Optical Materials*, **33**, 170 (2010).
57. J. Huang, X. Hu, J. Shen, D. Wu, C. Yin, R. Xiang, C. Yang, X. Liang, and W. Xiang, *CrystEngComm*, **17**, 7079 (2015).
58. Y. K. Lee, J. S. Lee, J. Heo, W. B. Im, and W. J. Chung, *Optics Letters*, **37**, 3276 (2012).
59. L.-Y. Chen, W.-C. Cheng, C.-C. Tsai, J.-K. Chang, Y.-C. Huang, J.-C. Huang, and W.-H. Cheng, *Optics Express*, **22**, A671 (2014).
60. L.-Y. Chen, W.-C. Cheng, C.-C. Tsai, Y.-C. Huang, Y.-S. Lin, and W.-H. Cheng, *Optical Materials Express*, **4**, 121 (2014).
61. R. Zhang, H. Lin, Y. Yu, D. Chen, J. Xu, and Y. Wang, *Laser & Photonics Reviews*, **8**, 158 (2014).
62. D. Chen and Y. Chen, *Ceramics International*, **40**, 15325 (2014).
63. Y. K. Lee, Y. H. Kim, J. Heo, W. B. Im, and W. J. Chung, *Optics Letters*, **39**, 4084 (2014).
64. Q.-Q. Zhu, X. Xu, L. Wang, Z.-F. Tian, Y.-Z. Xu, N. Hirosaki, and R.-J. Xie, *Journal of Alloys and Compounds*, **702**, 193 (2017).
65. J. S. Lee, S. Unithrattil, S. Kim, I. J. Lee, H. Lee, and W. B. Im, *Optics Letters*, **38**, 3298 (2013).
66. Q.-Q. Zhu, X.-J. Wang, L. Wang, N. Hirosaki, T. Nishimura, Z.-F. Tian, Q. Li, Y.-Z. Xu, X. Xu, and R.-J. Xie, *Journal of Materials Chemistry C*, **3**, 10761 (2015).
67. Y. Kenichi, F. Hiroshi, I. Makoto, H. Masamichi, T. Kohsei, S. Hiroyo, X. Rong-Jun, and H. Naoto, *Japanese Journal of Applied Physics*, **56**, 060302 (2017).
68. X. Zhang, J. Yu, J. Wang, B. Lei, Y. Liu, Y. Cho, R.-J. Xie, H.-W. Zhang, Y. Li, Z. Tian, Y. Li, and Q. Su, *ACS Photonics*, **4**, 986 (2017).
69. H. Chen, H. Lin, J. Xu, B. Wang, Z. Lin, J. Zhou, and Y. Wang, *Journal of Materials Chemistry C*, **3**, 8080 (2015).
70. R. Zhang, B. Wang, W. Zhu, C. Li, and H. Wang, *Journal of Alloys and Compounds*, **720**, 340 (2017).
71. C. S. McCamy, *Color Research & Application*, **17**, 142 (1992).
72. W. Davis and Y. Ohno, in *Proc. SPIE 5941, Fifth International Conference on Solid State Lighting*, p. 59411G 1 (2005).
73. S. Yi, W. J. Chung, and J. Heo, *Journal of the American Ceramic Society*, **97**, 342 (2014).
74. Y. Zhou, D. Chen, W. Tian, and Z. Ji, *Journal of the American Ceramic Society*, **98**, 2445 (2015).
75. H.-A. Park, Y. K. Lee, W. B. Im, J. Heo, and W. J. Chung, *Optical Materials*, **41**, 67 (2015).
76. S. Feng, H. Qin, G. Wu, H. Jiang, J. Zhao, Y. Liu, Z. Luo, J. Qiao, and J. Jiang, *Journal of the European Ceramic Society*, **37**, 3403 (2017).
77. X. Zhang, J. Yu, J. Wang, C. Zhu, J. Zhang, R. Zou, B. Lei, Y. Liu, and M. Wu, *ACS Applied Materials & Interfaces*, **7**, 28122 (2015).
78. K. Han, S. H. Lee, Y. G. Choi, W. B. Im, and W. J. Chung, *Journal of Non-Crystalline Solids*, **445**, 77 (2016).
79. S. H. Ahn, Y. H. Nam, K. Han, W. B. Im, K. Y. Cho, and W. J. Chung, *Journal of the American Ceramic Society*, **100**, 1280 (2017).
80. J. Zhong, D. Chen, Y. Zhou, Z. Wan, M. Ding, W. Bai, and Z. Ji, *Dalton Transactions*, **45**, 4762 (2016).
81. J. Zhong, D. Chen, Y. Zhou, Z. Wan, M. Ding, and Z. Ji, *Journal of the European Ceramic Society*, **36**, 1705 (2016).
82. B. Wang, H. Lin, J. Xu, H. Chen, and Y. Wang, *ACS Applied Materials & Interfaces*, **6**, 22905 (2014).
83. Z. Lin, H. Lin, J. Xu, F. Huang, H. Chen, B. Wang, and Y. Wang, *Journal of the European Ceramic Society*, **36**, 1723 (2016).
84. I. Pricha, W. Rossner, and R. Moos, *Journal of the American Ceramic Society*, **99**, 211 (2016).
85. Y. Peng, S. Wang, R. Li, H. Li, H. Cheng, M. Chen, and S. Liu, *Applied Optics*, **55**, 4933 (2016).
86. E. Kim, S. Unithrattil, I. S. Sohn, S. J. Kim, W. J. Chung, and W. B. Im, *Optical Materials Express*, **6**, 804 (2016).
87. Y. Peng, R. Li, H. Cheng, Z. Chen, H. Li, and M. Chen, *Journal of Alloys and Compounds*, **693**, 279 (2017).
88. I. Yamashita, H. Nagayama, and K. Tsukuma, *Journal of the American Ceramic Society*, **91**, 2611 (2008).
89. R. Boulesteix, A. Maître, J. F. Baumard, Y. Rabinovitch, and F. Reynaud, *Optics Express*, **18**, 14992 (2010).
90. S. Fujita, Y. Umayahara, and S. Tanabe, *Journal of the Ceramic Society of Japan*, **118**, 128 (2010).
91. Y. H. Kim, P. Arunkumar, and W. B. Im, *Ceramics International*, **41**, 5200 (2015).
92. Y. Kim, S. Kim, F. Iqbal, H. Yie, and H. Kim, *Optics Express*, **23**, A43 (2015).
93. S. Kim, H. Yie, S. Choi, A. Sung, and H. Kim, *Optics Express*, **23**, A1499 (2015).
94. Y. H. Song, G. S. Han, E. K. Ji, M.-J. Lee, Y. L. Song, D. S. Kong, M. K. Jung, B. W. Jeong, H. S. Jung, and D.-H. Yoon, *Journal of Materials Chemistry C*, **3**, 6148 (2015).
95. E. Kim, H. W. Shim, S. Unithrattil, Y. H. Kim, H. Choi, K.-J. Ahn, J. S. Kwak, S. Kim, H. Yoon, and W. B. Im, *ACS Nano*, **10**, 238 (2016).
96. Y.-P. Chang, J.-K. Chang, W.-C. Cheng, Y.-Y. Kuo, C.-N. Liu, L.-Y. Chen, and W.-H. Cheng, *Optical Materials Express*, **7**, 1029 (2017).
97. S. Li, Q. Zhu, D. Tang, X. Liu, G. Ouyang, L. Cao, N. Hirosaki, T. Nishimura, Z. Huang, and R.-J. Xie, *Journal of Materials Chemistry C*, **4**, 8648 (2016).

98. Y. R. Tang, S. M. Zhou, X. Z. Yi, H. Lin, S. Zhang, and D. M. Hao, *Optics Letters*, **40**, 5479 (2015).

99. Y. H. Kim, P. Arunkumar, B. Y. Kim, S. Unithrattil, E. Kim, S.-H. Moon, J. Y. Hyun, K. H. Kim, D. Lee, J.-S. Lee, and W. B. Im, *Nature Materials*, **16**, 543 (2017).

100. A. Lenef, J. Kelso, M. Tchoul, O. Mehl, J. Sorg, and Y. Zheng, in *SPIE Optical Engineering + Applications*, p. 91900C (2014).

101. H. Yoo, Y. Kouhara, H. C. Yoon, S. J. Park, J. H. Oh, and Y. R. Do, *RSC Advances*, **6**, 111640 (2016).

102. M. Faheem and K. Lynn, *American Journal of Analytical Chemistry*, **05**(11), 6 (2014).

103. M. Mikami, H. Watanabe, K. Uheda, and N. Kijima, *MRS Proceedings*, **1040** (2007).